Supplementary Information Appendix

Effects of fossil fuel and total anthropogenic emission removal on public health and climate

J. Lelieveld[a,b] , K. Klingmüller[a], A. Pozzer[a], R. T. Burnett[c], A. Haines[d], and V. Ramanathan[e]

[a]Max Planck Institute for Chemistry, 55128 Mainz, Germany; [b] The Cyprus Institute, 1645 Nicosia, Cyprus; [c]Population Studies Division, Health Canada, Ottawa, ON K1A 0K9, Canada; [d]London School of Hygiene and Tropical Medicine, London WC1 9SH, UK; [e]Scripps Institution of Oceanography, University of California, San Diego, La Jolla, CA 92093-0221, USA

Supplementary text

SI Methods

Global EMAC model: We used the global ECHAM/MESSy Atmospheric chemistry – Climate (EMAC) model, which comprehensively simulates atmospheric chemical and meteorological processes and interactions with the oceans and the biosphere (52,53). EMAC was developed at the Max Planck Institute for Chemistry in Mainz, building on the ECHAM atmosphere-ocean climate model of the Max Planck Institute for Meteorology in Hamburg (54,55), which has been modularized, and to which improved submodels and updates of boundary layer, radiation, cloud and convection routines have been introduced (56,57,58). The EMAC model development is coordinated within an international consortium: see https://www.messy-interface.org. Through this website additional model description, references and model output are available, and the software is publicly available through a community end-user license agreement. EMAC can be used for historical and present-day calculations as well as future projections. It couples atmosphere, ocean and land processes to simulate biogeochemical cycles of reactive compounds (59,60). It can be seen as an Earth system chemistry model, which can cover a wide range of space and time scales, typically up to decades with comprehensive chemistry and up to centuries with simplified chemistry schemes.

The model can be applied at various horizontal resolutions (between 0.5° and 2.8° latitude/ longitude, i.e. from about 50 km to 250 km grid spacing), and has a vertical range up to 80 km altitude, covering the lower and middle atmosphere (61,62). Here we applied EMAC at T63/L31 spatial resolution, i.e., at a spherical spectral truncation of T63 and a quadratic Gaussian grid spacing of about 1.85° latitude and longitude, and 31 hybrid terrain-following pressure levels up to 10 hPa in the lower stratosphere. Air quality and climate forcing calculations were performed with prescribed sea surface temperatures over a period of 25 years, of which the first five were dismissed as spin-up. Subsequently, the coupled atmosphere-ocean version of EMAC was used over 35 years (the first five

dismissed as spin-up), with the same comprehensive atmospheric chemistry and aerosol schemes, to compute equilibrium climate responses. This setup allows the atmosphere to restore radiative balance through heat exchange with the oceans, but does not enable transient climate change simulations based on time dependent emission scenarios. Here we pursue two simple scenarios by assuming the phase-out from fossil fuels and of all anthropogenic pollution sources in order to study the near-term climate responses. To differentiate between the effects of short-lived climate pollutants, we first performed two simulations in which aerosols from both source categories were removed, and subsequently two in which aerosols as well as greenhouse gases were removed.

Model setup: We have used EMAC to investigate the combined global impacts of air pollution on climate and public health. The various submodels represent tropospheric and lower stratospheric processes and their interaction with oceans, land and human influences, and they describe emissions, including isotopic composition, radiative processes, atmospheric multiphase chemistry, aerosol and deposition mechanisms (63,64,65,66,67,68). In our idealized sensitivity calculations, we removed fossil fuel related and all anthropogenic emissions. The latter category does not include the anthropogenic fraction of desert dust (13), which would require assumptions on land use change, and 10% of biomass burning emissions, which are considered natural, i.e., from fires that are ignited by lightning and difficult to extinguish (14). The anthropogenic sources include agriculture (e.g. NH_3, CH_4) to illustrate their impact on health and of maximum achievable emission reductions. For CH_4 we adopted pre-calculated concentration changes based on the tagging of source categories (67). One could argue that the instantaneous removal of emissions is not realistic from a future scenario perspective, but it demonstrates their large health impacts, while the climate simulations are not sensitive to the time period of the phase-out, at least not within this century (see Discussion). The health impacts may have some time dependency, as the population size, nutritional and medical care conditions can change in time. Therefore, we also present sensitivity calculations for the projected population of 2050.

EMAC simulates gas-phase and heterogeneous chemistry through the MECCA submodel, which accounts for the photochemical oxidation of natural and anthropogenic emissions, including a comprehensive account of volatile organic carbon compounds (69). Aerosol microphysics processes and gas/aerosol partitioning are simulated with the GMXe submodel (70,71,72). The aerosol size distribution is described by seven interacting lognormal modes (four hydrophilic and three hydrophobic). The aerosol composition within each mode is uniform (internally mixed), though can vary between modes (externally mixed). The hydrophilic size modes encompass the full aerosol size spectrum (nucleation, Aitken, accumulation and coarse), whereas the hydrophobic mode does not represent nucleation. The inorganic aerosol composition is computed with the ISORROPIA-II thermodynamic equilibrium submodel (73). It calculates the gas/liquid/solid equilibrium partitioning of inorganic compounds and water. Aeolian dust components can exist in the form of mineral salts in the solid phase and ions in the aqueous phase (74,75). The composition and atmospheric evolution of

organic aerosol compounds are simulated with the ORACLE submodel, which represents volatility classes of organics through their effective saturation concentrations (76). It accounts for primary and secondary combustion products from biomass burning, biofuel and fossil fuel use, including their chemical oxidation during atmospheric transport, which in turn influences the phase state of the particles.

Desert dust aerosols: Analogous to the chemical processing of inorganic and organic aerosols, atmospheric "ageing" has been introduced for aeolian dust particles (74,77). Especially the uptake of nitric acid, but also of other acids, can substantially influence the lifetime and climate properties of dust, which is the globally most abundant aerosol type. Neutralization reactions with mineral cations change the hygroscopicity of dust aerosols and their ability to act as cloud condensation nuclei (CCN). This has consequences for the aerosol optical depth (AOD) through water uptake, i.e., from being dry dust particles they become aqueous droplets, which in turn affects optical properties, dry and wet deposition processes. In EMAC the role of dust particles in cloud droplet formation is calculated with the "unified dust activation" scheme, which considers inherent hydrophilicity from water vapor absorption and acquired hygroscopicity from soluble salts formed through chemical ageing (29). We find that aged dust increases the cloud droplet number concentration near the source areas (by providing additional CCN) and decreases them over polluted areas by providing large CCN that are more effective in forming cloud droplets than small pollution aerosols. The dust aerosol radiative forcing is dominated by the former effect, which contributes to regional cooling (28,29). Recently, the ice nucleation parameterization has been revised to account for dust, black carbon, bioaerosols and organics (78).

Model evaluation: EMAC model results for the past decades have been extensively tested against measurement data of gases and particles from ground-based air quality networks and global observations from satellites (61–79). For global and regional evaluation of model simulated ozone we refer to Jöckel et al. (52,53) and Yan et al (80), and of AOD and $PM_{2.5}$ to Pozzer et al. (65,68,79,81). Recent model updates of aeolian dust and organic aerosols, including evaluation against measurement data, can be found in Klingmüller et al. (75) and Tsimpidi et al. (76), respectively. As an example, Fig. S1 shows the satellite-observed and modelled AOD at two wavelengths to distinguish the relatively large dust particles (10 μm data) from pollution aerosols (550 nm data). The performance of the climate model basic to EMAC has been evaluated by Roeckner et al. (54,82), with updates by Tost et al. (56,57) and Ouwersloot et al. (58). Fig. S2 compares modeled with satellite observed rainfall patterns. Fig. S3 presents some additional evaluation of our $PM_{2.5}$ results by comparing with a satellite-derived $PM_{2.5}$ product often used in air quality and public health assessments (5,83). Recent Global Burden of Disease (GBD) studies have applied these data (9,84), which combine MODIS satellite observations with results from a chemical transport model to provide prior information for the AOD retrieval and to relate observed column AOD to $PM_{2.5}$ (at 35% relative humidity) near the surface. Further, Figure S3 shows a direct comparison of model results and AOD observed by

AERONET ground stations, including the daily variability at three locations that are regularly affected by dust events. In our studies we apply the global EMAC results, because a model allows for sensitivity and scenario calculations, so that excess mortality can be attributed to source categories. Notwithstanding the use of either satellite-derived or EMAC model simulated data for exposure to pollution concentrations, we obtained nearly identical results as the GBD studies for 2010 (4,84) and 2015 (9,85) (see also next section). A study that evaluated model calculations for Europe at different spatial resolutions (20 and 100 km) and against satellite data (10 km) concluded that model uncertainties contribute a small part to the overall uncertainty in mortality calculations (86).

Global exposure mortality model (GEMM): To estimate public health impacts from air pollution, the model simulations have been combined with hazard ratio functions that use annual mean pollution concentrations to assess long-term health outcomes, following the approach of Anenberg et al. (87), Lim et al. (84), Burnett et al. (88) and Lelieveld et al. (4,85). We implemented the new GEMM of Burnett et al. (10) to estimate health risks, leading to substantially higher attributable excess mortality compared to previous studies (2,9). Hitherto, e.g., for the Global Burden of Disease (GBD), the impacts of very high $PM_{2.5}$ concentrations based on studies of outdoor air pollution (above those observed in countries where epidemiological cohort studies were performed) have been supplemented by studies of household pollution in addition to active and second-hand smoking (2,9), from which exposures are much larger than outdoor air pollution studies alone. The new GEMM is based on studies of outdoor air pollution only, including a study from China, which now cover an extensive global exposure range (41 cohorts from 16 countries). Furthermore, the GEMM was also constructed for a broad group of mortality causes, incorporating all non-communicable diseases and lower respiratory infections (NCD+LRI). The sum of excess mortality predicted by the GEMM for the five causes of death examined by the GBD is less than that predicted by the NCD+LRI group, suggesting that other causes of death, not included in these five, are related to particle exposure. Data sets used as input, such as country level baseline mortality rates (y_o) and years of life lost (YLL_o) for the different disease categories and populations, have been adopted from the WHO Global Health Observatory (89), being representative of the year 2015. Population numbers (P) are from the United Nations Department of Economic and Social Affairs/Population Division (http://esa.un.org/unpd/wpp).

Excess mortality (ΔM) calculations have been performed using the expression $\Delta M = y_o \cdot AF \cdot P$, in which the attributable fraction $AF = [R(z) - 1)] / R(z)$, with $R(z)$ being the hazard ratio (10). $R(z)$ is a function of concentration that specifies exposure (dependent on location). The years of life lost are calculated with the same expression, substituting y_o by YLL_o. The value of $R(z)$ is calculated for different disease categories such as ischemic heart disease (IHD), chronic obstructive pulmonary disease (COPD), lower respiratory tract infections (LRI), cerebrovascular disease (CVD), lung cancer (LC), for different age classes above 25 years. We added the previously applied exposure-response function for LRIs in children (<5 years) (85). The new risk estimator of Burnett et al. (10) introduces a GEMM for all NCD, which includes IHD, COPD, CVD and LC as well as other, yet undefined

categories. Results (i.e., for all NCD plus LRI) are presented in the main text. Tables S1–S2 present the different disease categories and results for all countries. The 95% confidence intervals for the GEMM results are based on a normal distribution approximation (10), and for the additional LRI in children <5 years on 1,000 realizations of exposure response functions (88). The GEMM describes uncertainty based on bootstrap methods that incorporate both sampling and model shape uncertainty, described by Burnett et al. (10,90). For O_3, which is assumed to affect COPD, R(z) is estimated following Jerrett et al. (91), with updated coefficients that include recent cohort studies. Our global total estimate of the attributable excess mortality rate of 8.79 (95%CI 7.11–10.41) million per year compares to 8.9 (95%CI 7.5–10.3) million per year of Burnett et al. (10), being more than twice as high as the estimate of the Global Burden of Disease for 2015 (2,10). By applying 2050 population data, we find that the total excess mortality rate is 9.68 (95%CI 7.78 – 11.50) million per year, i.e., about 10% higher than for 2015. By removing fossil fuel generated emissions, we find an avoidable mortality of 3.61(95%CI 2.96–4.21) in 2015 and 3.52(95%CI 2.88–4.11) in 2050. Removing all anthropogenic emissions yields an avoidable rate of 5.55 (95%CI 4.52–6.52) million in 2015, and 5.62 (95%CI 4.56–6.61) in 2015 (Tables S1 and S2). Hence the total avoidable rates change little between the 2015 and 2050 population scenarios.

Limitations of mortality estimates: The GEMM estimates how many deaths could be avoided per year if the population is exposed to a lower counterfactual level than current, ambient concentrations of air pollution. Since separate risk functions are derived for age categories, the GEMM additionally incorporates the age structure of the population. When mortality is attributed to a risk factor such as air pollution, the relationship is not distinctive but statistical (in the case of car accidents, for example, excess mortality relates to individuals who can be identified). To provide a context, we complement mortality estimates by how many years of life are lost. It should be understood that the methodology used with the GEMM is the same as for the health effects of active smoking, obesity, etc. Hence, whatever limitations are relevant for outdoor air pollution, they also apply to other risk factors. Although clinical and public-health research has uncovered unambiguous connections between air pollution, disease and mortality, even at very low levels of exposure (3,92), continued studies are needed to disentangle the causes and effects. For example, the harmfulness of different types of particles, individually and in mixtures, is not completely understood (93). The GEMM assumes that $PM_{2.5}$ toxicity does not depend on the source of outdoor air pollution. While previous studies of exposure-response formulations assumed counterfactual (i.e., potential outcome) uncertainty distributions, in the GEMM this dependency has diminished by directly deriving the shape of the exposure-mortality association from very low to high levels of air pollution, being accounted for in several of the 41 cohort studies (10). The estimates of mortality from air pollution include 95% confidence intervals, which represent parameter uncertainty related to the data used in the calculations. However, there can be additional uncertainty from incomplete knowledge, i.e., epistemic uncertainty. This includes unaccounted confounding factors, misclassification of health data, or limited

representativeness of hazard ratio functions as they rely on data from a small number of countries (16 countries). The confounder problem can work in two directions, either by over-attributing air pollution deaths to disease categories, or by unaccounted air pollution impacts. We emphasize that the GEMM follows the conservative practice of GBD and WHO studies, by focusing on risk factors and diseases for which there is convincing evidence of a causal relationship (3,10).

Supplementary figures

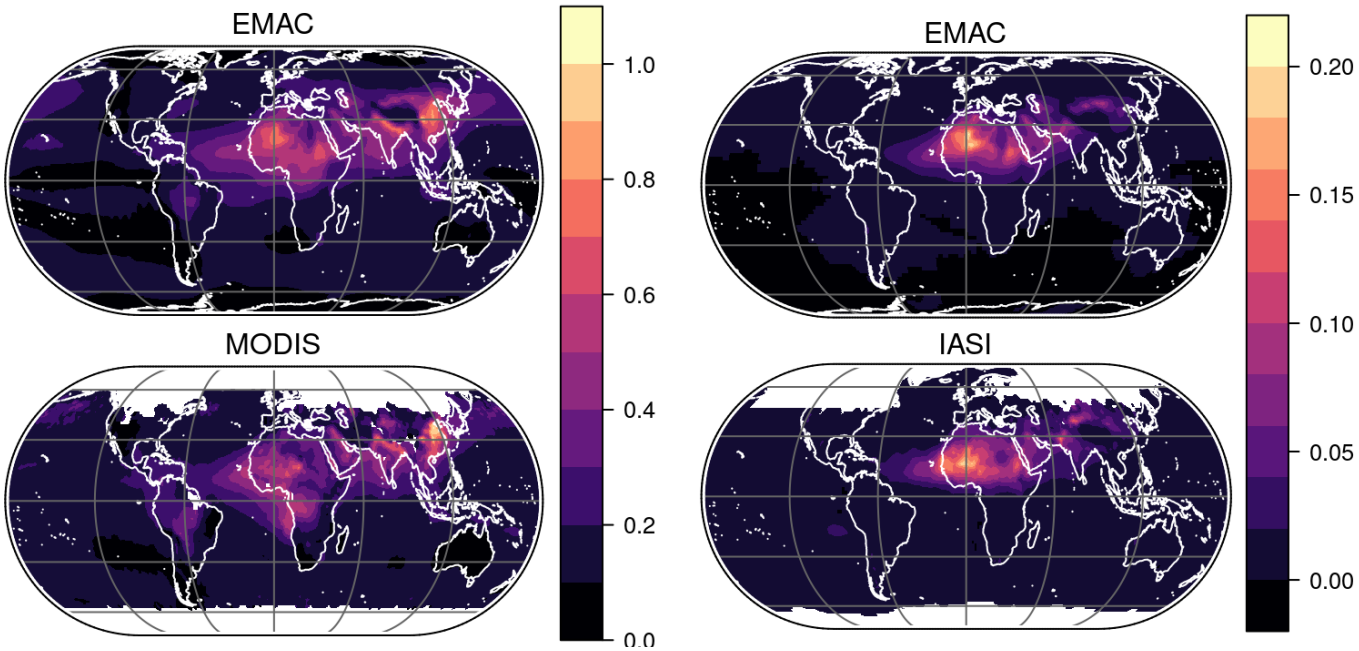

Supplementary Figure 1. EMAC model calculated and satellite observed aerosol optical depth (AOD) at 550 nm (left) and 10 µm (right) wavelength. The latter shows aeolian dust related aerosol optical depth. MODIS is the Moderate Resolution Imaging Spectroradiometer (NASA) and IASI the Infrared Atmospheric Sounding Interferometer (EUMETSAT).

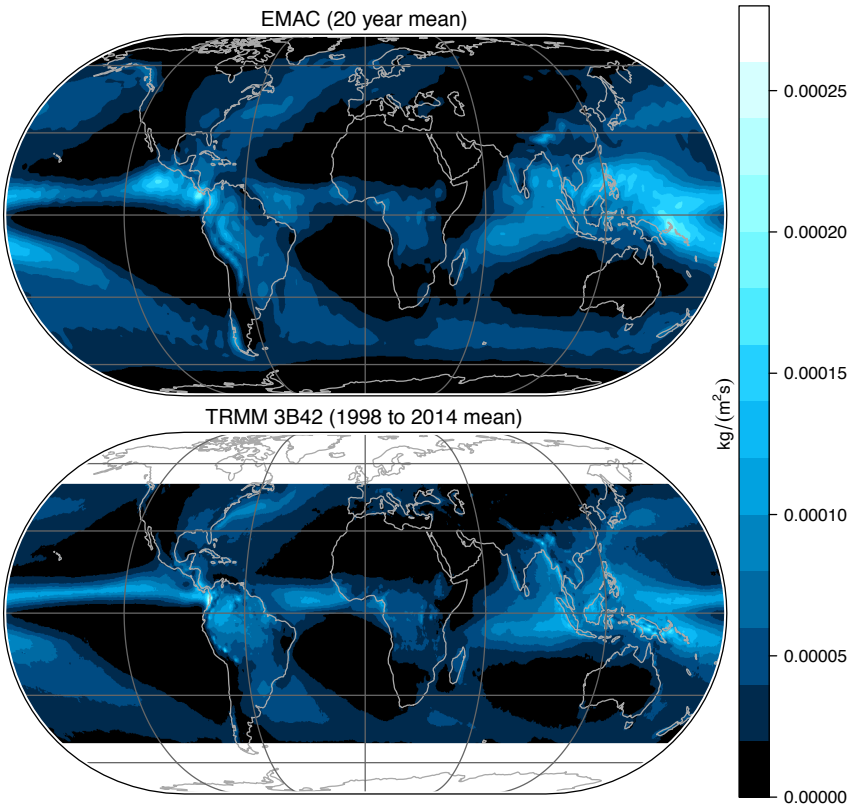

Supplementary Figure 2. EMAC model calculated annual precipitation, and that observed by the Tropical Rainfall Measuring Mission (TRMM) satellite.

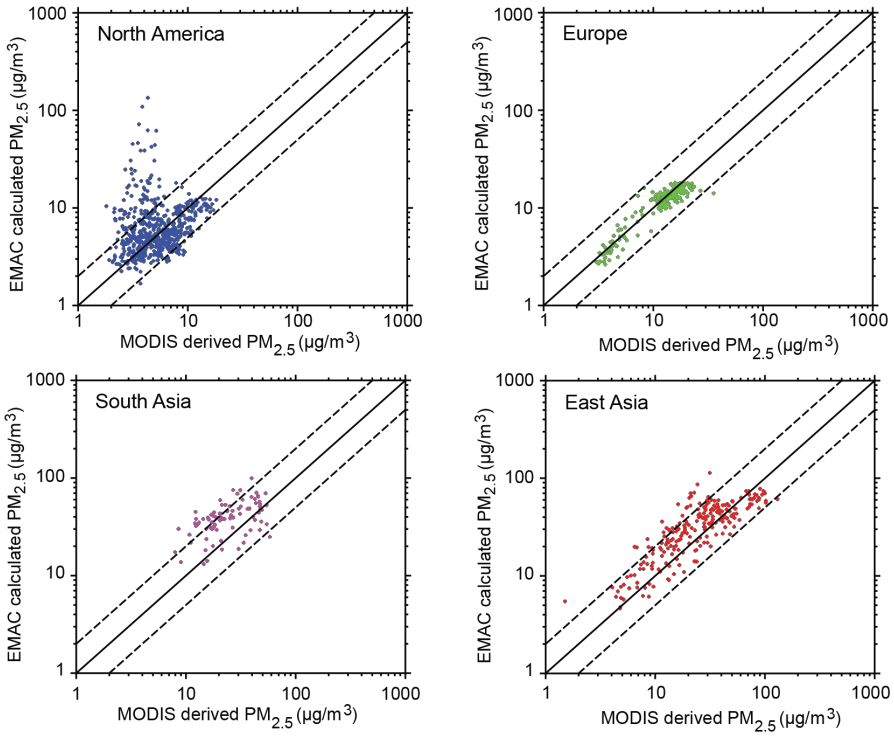

Supplementary Figure 3a. EMAC model calculated and MODIS satellite-derived mean $PM_{2.5}$ (at 35% relative humidity). The outliers (around 4 µg/m³ in MODIS data) in North America are related to forest fires in Canada, represented in the global fire emissions database (GFED) but not in the MODIS retrievals.

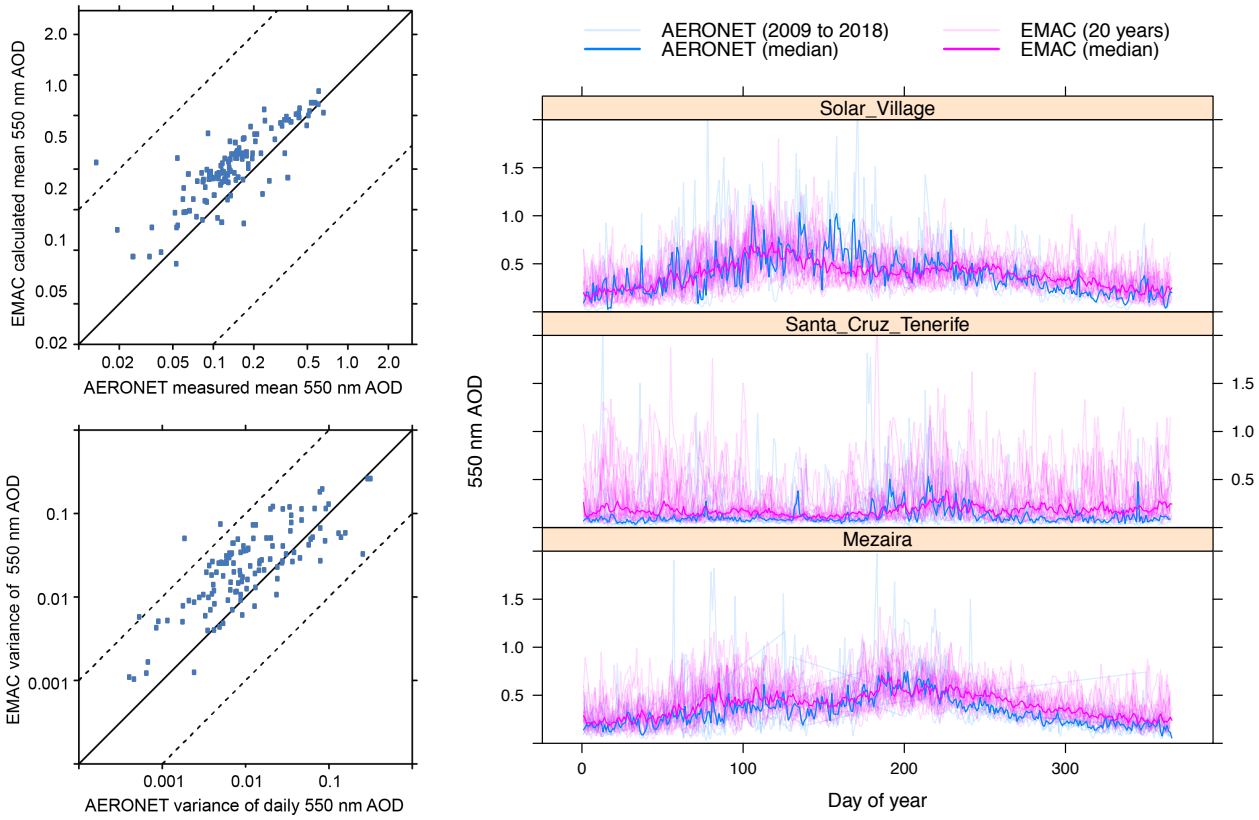

Supplementary Figure 3b. EMAC model calculated and AERONET observed aerosol optical depth for stations with at least two years of data during the 12 months between 2009 and 2018 (left), and for three dust-affected stations in the Middle East and North Africa (right). Some bias might be associated with the 24-hour EMAC averages and the cloud-free daytime observations of AERONET.

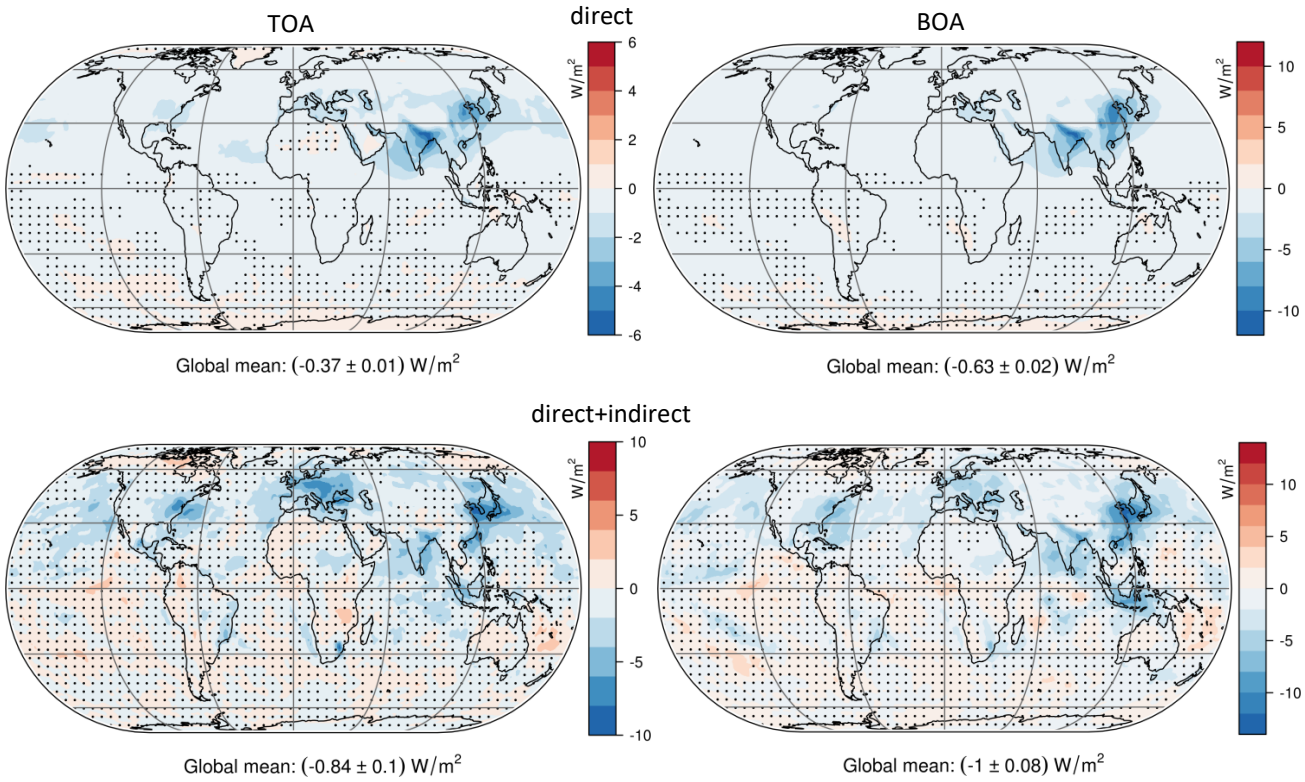

Supplementary Figure 4. Direct (top) and direct + indirect (bottom) radiative forcing of *fossil fuel related aerosols* at the TOA (left) and the BOA (right). Stippling denotes areas where radiative forcings are not significant at the 95% confidence level. Note that the direct aerosol effect typically has a higher statistical significance than indirect effects, as the latter influence clouds and rain, which are highly variable.

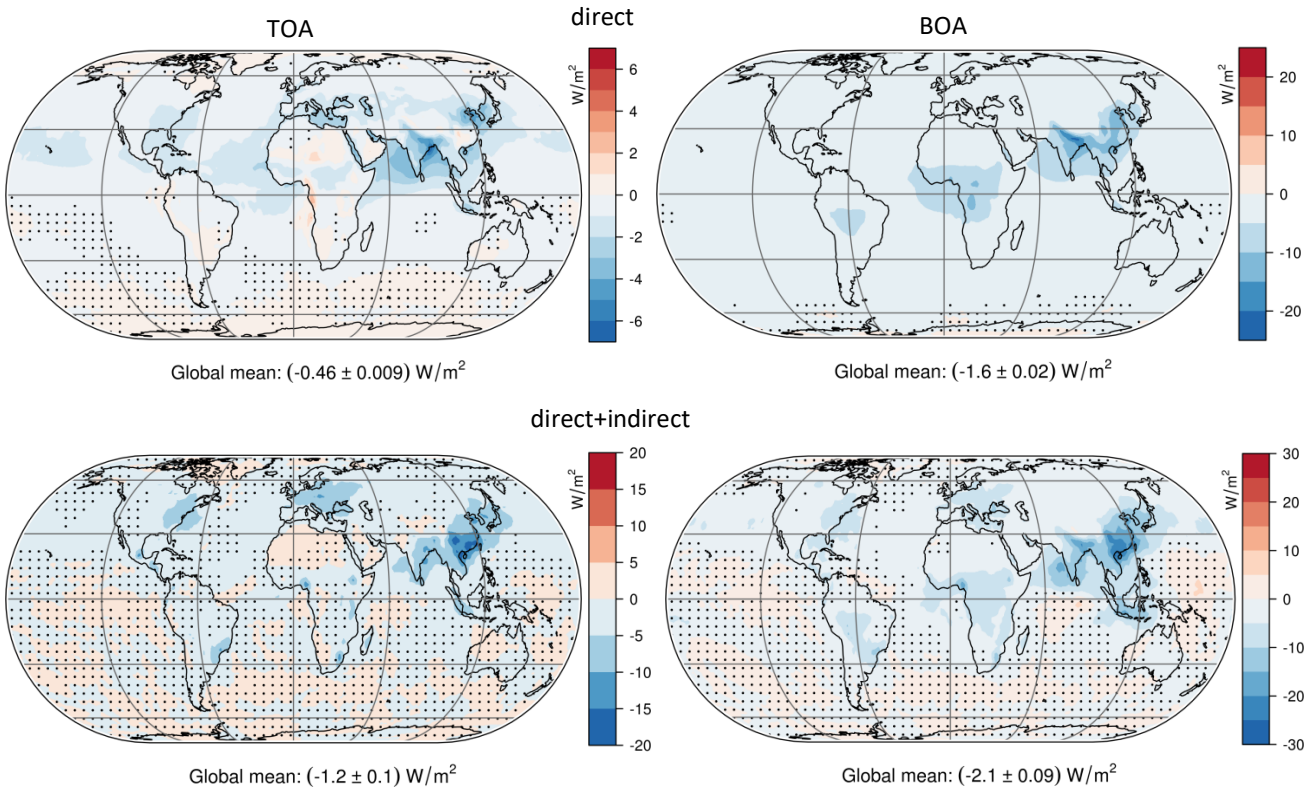

Supplementary Figure 5. Direct (top) and direct + indirect (bottom) radiative forcing of *all anthropogenic aerosols* at the TOA (left) and the bottom of the atmosphere (BOA, right). Stippling denotes areas where radiative forcings are not significant at the 95% confidence level. Note that the direct aerosol effect typically has a higher statistical significance than indirect effects, as the latter influence clouds and rain, being very variable.

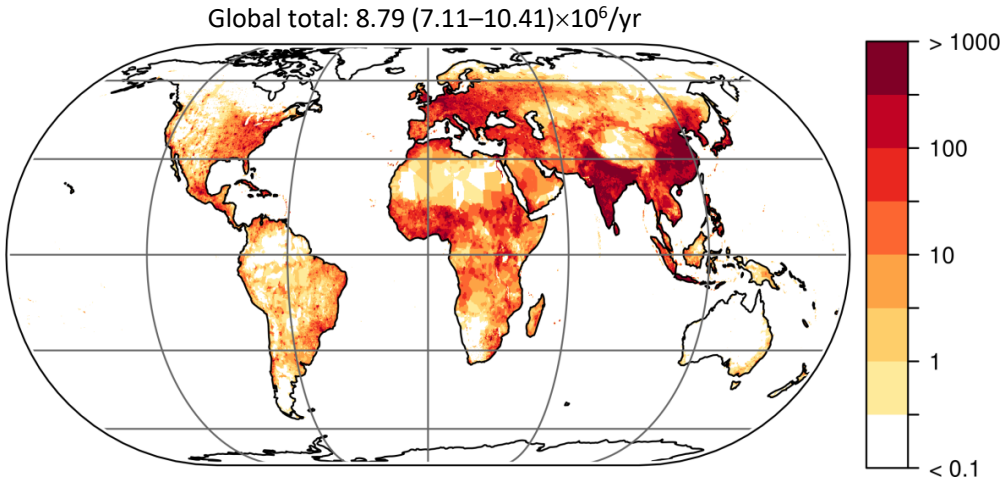

Supplementary Figure 6. Excess mortality rate attributed to air pollution.
Units: annual death rate per area of 1,000 km^2.

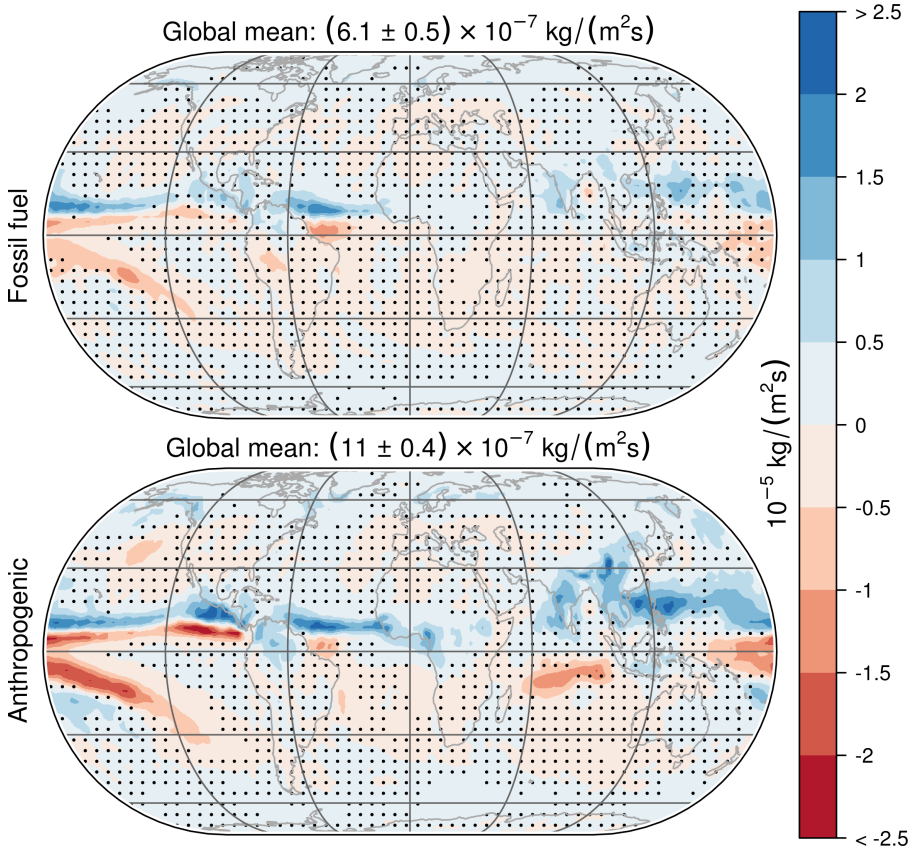

Supplementary Figure 7. Precipitation changes from removing particulate air pollution. Due to fossil fuel related (top), and due to all anthropogenic emissions (bottom). Stippling denotes areas where the precipitation changes are not significant at the 95% confidence level.

Supplementary tables

Table S1. Annual excess mortality rates attributed to air pollution in all countries. Excess deaths for disease categories, avoidable excess mortality, population data and unavoidable net warming from the phasing out of fossil fuel related and all anthropogenic emissions for air pollutants and greenhouse gases. Results are included for 2015 and 2050 population (same air pollution levels). Uncertainty ranges are given by the minimum and maximum values. Data are available in an attached excel file.

Table S2. Annual YLL attributed to air pollution in all countries. YLL for disease categories, avoidable YLL, population data and unavoidable net warming from the phasing out of fossil fuel related and all anthropogenic emissions for air pollutants and greenhouse gases. Results are included for 2015 and 2050 population (same air pollution levels). Uncertainty ranges are given by the minimum and maximum values. Data are available in an attached excel file.

References

52. Jöckel P, et al. (2006) The atmospheric chemistry general circulation model ECHAM5/MESSy: Consistent simulation of ozone from the surface to the mesosphere. *Atmos Chem Phys* 6:5067–5104.
53. Jöckel P, et al. (2010) Development cycle 2 of the Modular Earth Submodel System (MESSy2). *Geosci Model Dev* 3:717–752.
54. Roeckner E, et al. (2006) Sensitivity of simulated climate to horizontal and vertical resolution in the ECHAM5 atmosphere model. *J Clim* 19:3771–3791.
55. Marsland S, Haak H, Jungclaus JH, Latif M, Röske F (2003) The Max- Planck-Institute global ocean/sea ice model with orthogonal curvilinear coordinates. *Ocean Model* 5:91–127.
56. Tost H, Jöckel P, Lelieveld J (2006) Influence of different convection parameterizations in a GCM. *Atmos Chem Phys* 6:5475–5493.
57. Tost H, et al. (2007) Global cloud and precipitation chemistry and wet deposition: tropospheric model simulations with ECHAM5/MESSy1. *Atmos Chem Phys* 7:2733–2757.
58. Ouwersloot HG, Pozzer A, Steil B, Tost H, Lelieveld J (2015) Revision of convective transport in the EMAC atmospheric chemistry-climate model. *Geosci Model Dev* 8:2435–2445.
59. Ganzeveld LN, et al. (2010) The impact of land use and land cover changes on atmospheric chemistry-climate interactions. *J Geophys Res* 115:D23301.
60. Pozzer A, Jöckel P, Kern B, Haak H (2011) The atmosphere-ocean general circulation model EMAC-MPIOM. *Geosci Model Develop* 4:771–784.
61. Lelieveld J, et al. (2007) Stratospheric dryness: model simulations and satellite observations. *Atmos Chem Phys* 7:1313–1332.
62. Brühl C, Lelieveld J, Tost H, Höpfner M, Glatthor N (2015) Stratospheric sulfur and its implications for radiative forcing simulated by the chemistry climate model EMAC. *J Geophys Res* 120:2103–2118.
63. Kerkweg A, Sander R, Tost H, Jöckel P (2006) Technical note: Implementation of prescribed (OFFLEM), calculated (ONLEM), and pseudo-emissions (TNUDGE) of chemical species in the Modular Earth Submodel System (MESSy). *Atmos Chem Phys* 6:3603–3609.
64. Tost H, Jöckel P, Kerkweg A, Sander R, Lelieveld J. (2006) Technical note: A new comprehensive SCAVenging submodel for global atmospheric chemistry modelling. *Atmos Chem Phys* 6:565–574.
65. Pozzer A, et al. (2010) Observed and simulated global distribution and budget of atmospheric C2-C5 alkanes, *Atmos Chem Phys* 10:4403–4422.
66. Klingmüller K, Steil B, Brühl C, Tost H, Lelieveld J (2014) Sensitivity of aerosol extinction to new mixing rules in the AEROPT submodel of the ECHAM5/MESSy1.9 atmospheric chemistry (EMAC) model. *Geosci Model Dev* 7:2503–2516.
67. Zimmermann PH, et al. (2018) Model simulations of atmospheric methane and their evaluation using AGAGE/NOAA surface- and IAGOS-CARIBIC aircraft observations, 1997-2014. *Atmos Chem Phys Discuss*, https://doi.org/10.5194/acp-2017-1212.
68. Pozzer A, et al. (2015) AOD trends during 2001–2010 from observations and model simulations. *Atmos Chem Phys* 15:5521–5535.
69. Lelieveld J, Gromov S, Pozzer A, Taraborrelli D (2016) Global tropospheric hydroxyl distribution, budget and reactivity. *Atmos Chem Phys* 16:12477–12493.
70. Pringle KJ, et al. (2010) Description and evaluation of GMXe: A new aerosol submodel for global simulations (v1). *Geosci Model Dev* 3:391–412.
71. Pringle KJ, Tost H, Pozzer A, Pöschl U, Lelieveld J (2010) Global distribution of the effective hygroscopicity parameter for CCN activation. *Atmos Chem Phys* 10:5241–5255.
72. Pozzer A, et al. (2012) Distributions and regional budgets of aerosols and their precursors simulated with the EMAC chemistry-climate model. *Atmos Chem Phys* 12:961–987.
73. Fountoukis C, Nenes A (2007) ISORROPIA II: a computationally efficient thermodynamic equilibrium model for K^+–Ca^{2+}–Mg^{2+}–NH_4^+–Na^+–SO_4^{2-}–NO_3^-–Cl^-–H_2O aerosols. *Atmos Chem Phys* 7:4639–4659.
74. Karydis VA, Tsimpidi AP, Pozzer A, Astitha M, Lelieveld (2016). Effects of mineral dust on global atmospheric nitrate concentrations. *Atmos Chem Phys* 16:1491–1509.
75. Klingmüller K, et al. (2018) Revised mineral dust emissions in the atmospheric chemistry-climate model EMAC (based on MESSy 2.52). *Geosci Model Dev* 11:989–1008.
76. Tsimpidi A, Karydis V, Pozzer A, Pandis S, Lelieveld J (2018) ORACLE 2-D (v2.0): an efficient module to compute the volatility and oxygen content of organic aerosol with a global chemistry – climate model. *Geosci Model Dev* 11:3369-3389.

77. Abdelkader M, et al. (2017) Chemical aging of atmospheric mineral dust during transatlantic transport. *Atmos Chem Phys* 17:3799–3821.
78. Bacer S, et al. (2018) Implementation of a comprehensive ice crystal formation parameterization for cirrus and mixed-phase clouds into the EMAC model (based on MESSy 2.53). *Geosci Model Dev* 11:4021-4041.
79. Pozzer A, Tsimpidi A, Karydis V, de Meij A, Lelieveld J (2017) Impact of agricultural emissions on fine particulate matter and public health. *Atmos Chem Phys* 17:12813–12826.
80. Yan Y, Pozzer A, Ojha N, Lin J, Lelieveld, J (2018) Analysis of European ozone trends in the period 1995–2014. *Atmos Chem Phys* 18:5589−5605.
81. de Meij A, Pozzer A, Pringle KJ, Tost H, Lelieveld J (2012) EMAC model evaluation and analysis of atmospheric aerosol properties and distribution. *Atmos Res* 114-115:38–69.
82. Hagemann S, Arpe K, Roeckner E (2006) Evaluation of the hydrological cycle in the ECHAM5 model. *J Clim* 19:3810–3827.
83. van Donkelaar A, et al. (2016) Global estimates of fine particulate matter using a combined geophysical-statistical method with information from satellites, models, and monitors. *Environ Sci Technol* 50:3762–3772.
84. Lim SS, et al. (2012) A comparative risk assessment of burden of disease and injury attributable to 67 risk factors and risk factor clusters in 21 regions, 1990–2010: a systematic analysis for the Global Burden of Disease Study 2010. *Lancet* 380:2224–2260.
85. Lelieveld J, Haines A, Pozzer A (2018) Age-dependent health risk from ambient air pollution: a modelling and data analysis of childhood mortality in middle-income and low-income countries. *Lancet Planet Health* 2:e292-300.
86. Kushta J, Pozzer A, Lelieveld J (2018) Uncertainties in estimates of mortality attributable to ambient PM2.5 in Europe. *Environ Res Lett* 13:064029.
87. Anenberg SC, Horowitz LW, Tong DQ, West JJ (2010) An estimate of the global burden of anthropogenic ozone and fine particulate matter on premature human mortality using atmospheric modelling. *Environ Health Perspect* 118:1189–1195.
88. Burnett RT, et al. (2014) An integrated risk function for estimating the Global Burden of Disease attributable to ambient fine particulate matter exposure. *Environ Health Perspect* 122:397–403.
89. World Health Organization (WHO) (2017) Global Health Observatory (Dept of Information, Evidence and Research, WHO, Geneva, Switzerland). Available at http://www.who.int/gho/database/en/
90. Nasari M et al., (2015). A class of non-linear exposure-response models suitable for health impact assessment applicable to large cohort studies of ambient air pollution. Air quality, atmosphere, and health: DOI: 10.1007/s11869-016-0398-z.
91. Jerrett M, et al. (2009) Long-term ozone exposure and mortality. *N Engl J Med* 360:1085–1095.
92. Di Q, et al. (2017) Air pollution and mortality in the medicare population. *N Engl J Med* 376:2513–2522.
93. West JJ, et al. (2016) What we breathe impacts our health: Improving understanding of the link between air pollution and health. *Environ Sci Technol* 50:4895–4904.